Divergent roles of haptoglobin and hemopexin deficiency for disease progression of Shiga-toxin–induced hemolytic-uremic syndrome in mice

see commentary on page 1107

OPEN

Wiebke Pirschel[1,2,9], Antonio N. Mestekemper[1,2,9], Bianka Wissuwa[1,2], Nadine Krieg[1,2], Sarah Kröller[1,2], Christoph Daniel[3], Florian Gunzer[4], Emanuela Tolosano[5], Michael Bauer[1,6], Kerstin Amann[3], Stefan H. Heinemann[7,8] and Sina M. Coldewey[1,2,6]

[1]Department of Anesthesiology and Intensive Care Medicine, Jena University Hospital, Jena, Germany; [2]Septomics Research Center, Jena University Hospital, Jena, Germany; [3]Department of Nephropathology, Friedrich-Alexander University (FAU) Erlangen-Nürnberg, Erlangen, Germany; [4]Department of Hospital Infection Control, University Hospital Carl Gustav Carus, TU Dresden, Dresden, Germany; [5]Department of Molecular Biotechnology and Health Sciences, Molecular Biotechnology Center, University of Torino, Torino, Italy; [6]Center for Sepsis Control and Care (CSCC), Jena University Hospital, Jena, Germany; [7]Center of Molecular Biomedicine (CMB), Department of Biophysics, Friedrich Schiller University Jena, Jena, Germany; and [8]Center of Molecular Biomedicine (CMB), Department of Biophysics, Jena University Hospital, Jena, Germany

Thrombotic microangiopathy, hemolysis and acute kidney injury are typical clinical characteristics of hemolytic-uremic syndrome (HUS), which is predominantly caused by Shiga-toxin–producing *Escherichia coli*. Free heme aggravates organ damage in life-threatening infections, even with a low degree of systemic hemolysis. Therefore, we hypothesized that the presence of the hemoglobin- and the heme-scavenging proteins, haptoglobin and hemopexin, respectively impacts outcome and kidney pathology in HUS. Here, we investigated the effect of haptoglobin and hemopexin deficiency (haptoglobin$^{-/-}$, hemopexin$^{-/-}$) and haptoglobin treatment in a murine model of HUS-like disease. Seven-day survival was decreased in haptoglobin$^{-/-}$ (25%) compared to wild type mice (71.4%), whereas all hemopexin$^{-/-}$ mice survived. Shiga-toxin–challenged hemopexin$^{-/-}$ mice showed decreased kidney inflammation and attenuated thrombotic microangiopathy, indicated by reduced neutrophil recruitment and platelet deposition. These observations were associated with supranormal haptoglobin plasma levels in hemopexin$^{-/-}$ mice. Low dose haptoglobin administration to Shiga-toxin–challenged wild type mice attenuated kidney platelet deposition and neutrophil recruitment, suggesting that haptoglobin at least partially contributes to the beneficial effects. Surrogate parameters of hemolysis were elevated in Shiga-toxin–challenged wild type and haptoglobin$^{-/-}$ mice, while signs for hepatic hemoglobin degradation like heme oxygenase-1, ferritin and CD163 expression were only increased in Shiga-toxin–challenged wild type mice. In line with this observation, haptoglobin$^{-/-}$ mice displayed tubular iron deposition as an indicator for kidney hemoglobin degradation. Thus, haptoglobin and hemopexin deficiency plays divergent roles in Shiga-toxin–mediated HUS, suggesting haptoglobin is involved and hemopexin is redundant for the resolution of HUS pathology.

Kidney International (2022) **101,** 1171–1185; https://doi.org/10.1016/j.kint.2021.12.024

KEYWORDS: acute kidney injury; haptoglobin; hemolysis; hemolytic-uremic syndrome; hemopexin; iron homeostasis; Shiga toxin

Translational Statement

Hemolytic-uremic syndrome is a life-threatening complication of infection with enterohemorrhagic *Escherichia coli* and is characterized by microangiopathic hemolytic anemia and renal impairment. Evidence suggests that free heme contributes to disease progression in systemic inflammation. We show that the hemoglobin and heme scavenger proteins haptoglobin and hemopexin play divergent roles in hemolytic-uremic syndrome pathogenesis. Our data indicate that hemopexin is redundant for the resolution of hemolytic-uremic syndrome pathology while haptoglobin deficiency aggravates disease progression in mice with hemolytic-uremic syndrome, and higher endogenous haptoglobin levels as well as haptoglobin administration are associated with an attenuation of surrogate parameters of thrombotic microangiopathy and inflammation.

Correspondence: *Sina M. Coldewey, Department of Anesthesiology and Intensive Care Medicine, Jena University Hospital, Am Klinikum 1, 07747 Jena, Germany. E-mail: sina.coldewey@med.uni-jena.de*

[9]These authors have contributed equally to this work.

Received 23 February 2021; revised 5 December 2021; accepted 16 December 2021; published online 11 January 2022

Hemolytic-uremic syndrome (HUS) is a rare but severe systemic complication upon infection with Shiga-toxin (Stx)–producing enterohemorrhagic *Escherichia coli* (STEC). STEC-HUS, a thrombotic microangiopathy (TMA)

primarily affecting the kidneys, is clinically characterized by hemolytic anemia, thrombocytopenia, and end-organ damage caused by thrombosis in small blood vessels.[1] It is the most frequent reason for acute kidney injury in childhood,[2] but severe HUS courses have also been described in adults.[3,4] Although the pathogenesis is still under investigation,[5] it is evident that Stx, comprising Stx1 and Stx2, is the major virulence factor of STEC.[6] By binding to globotriaosylceramide receptor with high affinity and interfering with protein synthesis, Stx leads to epithelial and endothelial cell damage, thereby initiating the occurrence of TMA in the kidneys.[6] Clot deposition in the microvasculature leads to subsequent tissue ischemia, organ injury, and hemolysis.[1,6] Therapeutic options are currently supportive and dialysis is often required. Because there is no specific therapy, further studies are needed to evaluate potential targets for therapeutic approaches. Free heme is a known relevant factor in the maintenance of pathological processes in life-threatening infections by leading to inflammation,[7,8] complement activation,[9,10] and reactive oxygen species.[11] Recently, elevated free heme could be detected in the plasma of patients with STEC-HUS.[12] However, the effect of heme and heme degradation products on disease progression has not yet been investigated. In mammalians, clearance of cell-free hemoglobin (Hb) and heme-bound iron is mainly regulated by the scavenging systems haptoglobin (Hp) and hemopexin (Hx). Hp is the plasma protein with the highest binding affinity to Hb. As an acute phase protein, it is upregulated under inflammatory conditions and predominantly produced in hepatocytes.[13] Key functions of Hp are preventing glomerular filtration of Hb and enabling Hb degradation by the reticuloendothelial system, especially in the spleen and liver,[14,15] thereby protecting the kidneys from Hb-mediated cytotoxicity.[16] CD163, a membrane receptor on macrophages, binds to the Hp-Hb complex with high affinity and leads to its endocytosis.[15] In the absence of Hp, glomerular filtered Hb binds to the multiligand receptors megalin and cubilin mediating its tubular uptake.[17] When Hb becomes oxidized to methemoglobin, its heme groups dissociate and potentially exert cytotoxicity via the centrally bound iron.[18] Various plasma proteins such as albumin, α1-microglobulin (α1M), and Hx prevent iron-mediated damage by binding free heme.[18] Hx is the scavenging protein with the highest affinity to heme and a murine but not human acute phase protein mainly produced in the liver.[19,20] The Hx-heme complex is removed from the plasma by low-density lipoprotein receptor–related protein 1–mediated endocytosis.[21] After its uptake, the intracellular degradation of heme into equimolar amounts of ferrous iron (Fe^{2+}), carbon monoxide (CO), and biliverdin is mediated via the 2 heme oxygenase isoforms HO-1 and HO-2.[22] HO-1 is ubiquitously expressed and inducible and gains cytoprotective properties by modulating the tissue response in the presence of various stress factors.[22] First evidence from cell culture experiments suggest that Stx augments hemin-mediated toxicity in renal epithelial cells, which can be attenuated by HO-1 induction.[23] Heme degradation by HO-1 increases the availability of free iron.[24] While biliverdin is converted to bilirubin by biliverdin reductase,[25] labile iron is rapidly bound by the intracellular iron storage protein ferritin to prevent reactive oxygen species formation.[26] Ferritin consists of a heavy (Fth1) and a light (Ftl1) chain; the former has ferroxidase activity being crucial for iron storage.[27] The transmembrane protein ferroportin (SCL40A1) mediates iron transport into the circulation where it is bound by transferrin.[28] Ferroportin expression is locally regulated by iron regulatory proteins and systemically by the acute phase protein hepcidin.[28]

Hitherto, the role of the Hb- and heme-scavenging proteins Hp and Hx in HUS pathology has not been addressed. We hypothesized that Hp and Hx affect the disease progression of STEC-HUS by ameliorating Hb- and heme-mediated cytotoxicity and kidney injury. Thus, we analyzed the effect of Hp and Hx deficiency as well as Hp treatment in a murine model of HUS-like disease. Elucidating the role of these proteins in STEC-HUS provides a deeper understanding of the pathogenesis and offers the potential to develop novel therapeutic strategies.

METHODS

Information on commercially available kits, buffers, and antibodies used in the study and other methodical details including methods relevant to Supplementary Results are provided in Supplementary Materials.

Animal experiments

Generation of $Hp^{-/-}$ and $Hx^{-/-}$ mice has been described in Lim *et al.*[29] and Tolosano *et al.*,[16] respectively. HUS was induced in 10- to 15-week-old male C57BL/6J wild-type (WT), $Hp^{-/-}$, and $Hx^{-/-}$ mice.[30] Mice were subjected to 25 ng/kg bodyweight Stx2 (WT Stx, $Hp^{-/-}$ Stx, and $Hx^{-/-}$ Stx) or 0.9% NaCl (WT sham, $Hp^{-/-}$ sham, and $Hx^{-/-}$ sham) i.v. on days 0, 3, and 6 accompanied by volume resuscitation with 800 μl of Ringer's lactate solution s.c. 3 times daily. Bodyweight and HUS score (Supplementary Table S1) were determined as described previously.[30] Survival was assessed up to day 7, or mice were killed when an HUS score of 4 (high-grade disease state) was reached to comply with ethical regulations. All further analyses were performed in samples obtained at day 5 after HUS induction. For Hp treatment, WT mice received 0.5 mg of Hp (ABIN491578, antibodies-online GmbH) in 200 μl of phosphate-buffered saline i.p. on days 0 and 3. All procedures were approved by the regional animal welfare committee (Thuringia State Office for Food Safety and Consumer Protection [TLLV], Bad Langensalza, Germany; registration number 02-040/16) and performed in accordance with the German legislation.

Plasma analysis

Blood withdrawal, plasma preparation, and analysis of hemolysis were performed as described previously.[30] α1M, albumin, Hp, Hx, urea, neutrophil gelatinase–associated lipocalin, bilirubin, and hepcidin plasma levels were analyzed with commercial kits according to manufactures instructions (Supplementary Table S2).

Histological and immunohistochemical analysis

Kidneys were histopathologically and immunohistochemically evaluated using periodic acid–Schiff, kidney injury molecule-1, CD31, F4-80, complement component 3 (C3c), cleaved caspase-3 (CC-3) staining as described previously,[30] as well as ferroportin, lymphocyte

antigen 6 complex, locus G, glycoprotein 1b, and iron staining (antibodies in Supplementary Tables S3 and S4).

Gene expression analysis

Isolation of RNA, performance of real-time polymerase chain reaction (Supplementary Table S5), and data analysis were described previously.[31,32]

Protein expression analysis

Immunoblot analysis was performed as described previously.[31] A total of 100 μg of total protein were used for the blotting of renal HO-1, and 25 μg of total protein were used for the blotting of Fth1, hepatic HO-1, and CD163 (antibodies in Supplementary Table S6). Proteins of interest were normalized to total protein load by using the stain-free technology (Bio-Rad Laboratories, Inc.). Bands with normalization factors <0.7 and >1.3 were excluded from the analysis.[33] Samples from 6 animals per group were pooled to equal protein amounts for the representative blots of renal HO-1 and Fth1. Individual blots (1 animal per group) are shown in Supplementary Figure S1. Data are presented relative to the mean of sham animals.

Statistics

Data were analyzed with Prism version 7.03 (GraphPad Software) and are depicted as median (interquartile range) for n observations. Survival was analyzed by generating Kaplan-Meier curves and evaluated by using the Mantel-Cox test. The Mann-Whitney U test was used to compare the Stx groups of each strain with the corresponding sham group, each knockout sham group with the WT sham group, and each knockout Stx group with the WT Stx group. A P value of <0.05 was considered significant.

RESULTS

Seven-day survival is worse in $Hp^{-/-}$ mice and improved in $Hx^{-/-}$ mice

The survival rate of Stx-challenged WT mice (71.4%) was decreased but not significantly altered compared to WT sham mice (100%; Figure 1a). Seven-day survival of Stx-challenged $Hp^{-/-}$ mice (25%) was lower than that of $Hp^{-/-}$ sham mice (100%). Most notably, all Stx-challenged $Hx^{-/-}$ mice survived (100%). Both Stx-challenged WT and $Hx^{-/-}$ mice showed significantly higher survival rates than did Stx-challenged $Hp^{-/-}$ mice.

The course of disease is more severe in $Hp^{-/-}$ and WT mice than in $Hx^{-/-}$ mice

Disease progression, indicated by increased HUS scores, was apparent in all Stx-challenged mice (Figure 1b). However, although HUS scores of Stx-challenged $Hp^{-/-}$ and WT mice were comparable on day 5, Stx-challenged $Hx^{-/-}$ mice showed less disease progression (Figure 1c). All Stx-challenged mice lost weight during the course of the disease (Figure 1d). Five days after HUS induction, weight loss of $Hp^{-/-}$ mice was higher than that of WT mice whereas weight loss of $Hx^{-/-}$ mice was comparable to WT mice (Figure 1e).

Expression of the Hb and heme scavenger proteins Hx, α1M, albumin, and Hp in WT, $Hp^{-/-}$, and $Hx^{-/-}$ mice

A compensatory upregulation of α1M in $Hx^{-/-}$ mice with sickle cell disease[34] as well as Hp in $Hx^{-/-}$ mice and Hx in $Hp^{-/-}$ mice with artificial hemolysis has been described.[35] Thus, we investigated plasma levels of Hb- and heme-binding proteins.

Hepatic *Hx* gene expression was increased in Stx-challenged WT and $Hp^{-/-}$ mice compared with their corresponding sham group (Figure 2a). A similar pattern was found for Hx plasma levels; furthermore, they were higher in $Hp^{-/-}$ sham mice than in WT sham mice (Figure 2b).

Plasma α1M levels were decreased in Stx-challenged WT mice but unchanged in $Hp^{-/-}$ and $Hx^{-/-}$ mice compared with their corresponding sham group (Figure 2c).

Heme-binding properties have been described for albumin.[36] However, plasma albumin levels were unchanged in Stx-challenged WT and knockout mice compared with their corresponding sham group (Figure 2d).

Hepatic *Hp* gene expression was increased in Stx-challenged WT and $Hx^{-/-}$ mice compared with their corresponding sham group (Figure 2e). A similar pattern was found for plasma Hp levels (Figure 2f). Notably, plasma Hp levels were higher in $Hx^{-/-}$ mice than in WT mice irrespective of Stx challenge.

Kidney impairment in WT, $Hp^{-/-}$, and $Hx^{-/-}$ mice

The liver, lung, colon, and kidneys of WT, $Hp^{-/-}$, and $Hx^{-/-}$ mice were assessed for morphological alterations. Although no relevant morphological changes appeared in the lung and colon, diffuse granulomatous changes were detected in liver sections of Stx-challenged mice and knockout sham animals (Supplementary Figures S2 and S3), accompanied by unchanged liver enzymes (Supplementary Figure S4).

All Stx-challenged genotypes showed severe kidney injury, indicated by increased urea (Figure 3a) and neutrophil gelatinase–associated lipocalin plasma levels (Figure 3b), altered morphology in periodic acid–Schiff–stained sections (Figure 3c; Supplementary Figure S5A), and elevated kidney injury molecule-1 expression (Figure 3d), suggesting that the kidney is the primarily affected organ in this murine model. Creatinine plasma levels were elevated in all Stx-challenged genotypes compared with their corresponding sham group and slightly increased in Stx-challenged $Hp^{-/-}$ mice compared with WT mice (Supplementary Figure S6A). Potassium plasma levels were elevated in Stx-challenged WT and $Hp^{-/-}$ mice but not in $Hx^{-/-}$ mice compared with their corresponding sham group (Supplementary Figure S6B). Furthermore, enhanced potassium levels were observed in Stx-challenged $Hp^{-/-}$ mice compared with WT mice.

In human STEC-HUS, glomerular damage is predominant but tubular damage also contributes to the pathology.[37] Ultrastructural analysis revealed severe tubular injury in all Stx-challenged mice but no alterations of podocytes (Supplementary Figure S7). Murine Stx models do not completely mimic human HUS. Several models have been developed to highlight certain aspects of HUS, comprising genetic modifications to study the lectin pathway[38] or enhance thrombotic processes[39] and coinjection of lipopolysaccharide[40] to provoke a broader range of HUS symptoms such as glomerular changes and thrombocytopenia. This study focuses on Stx-mediated pathomechanisms.

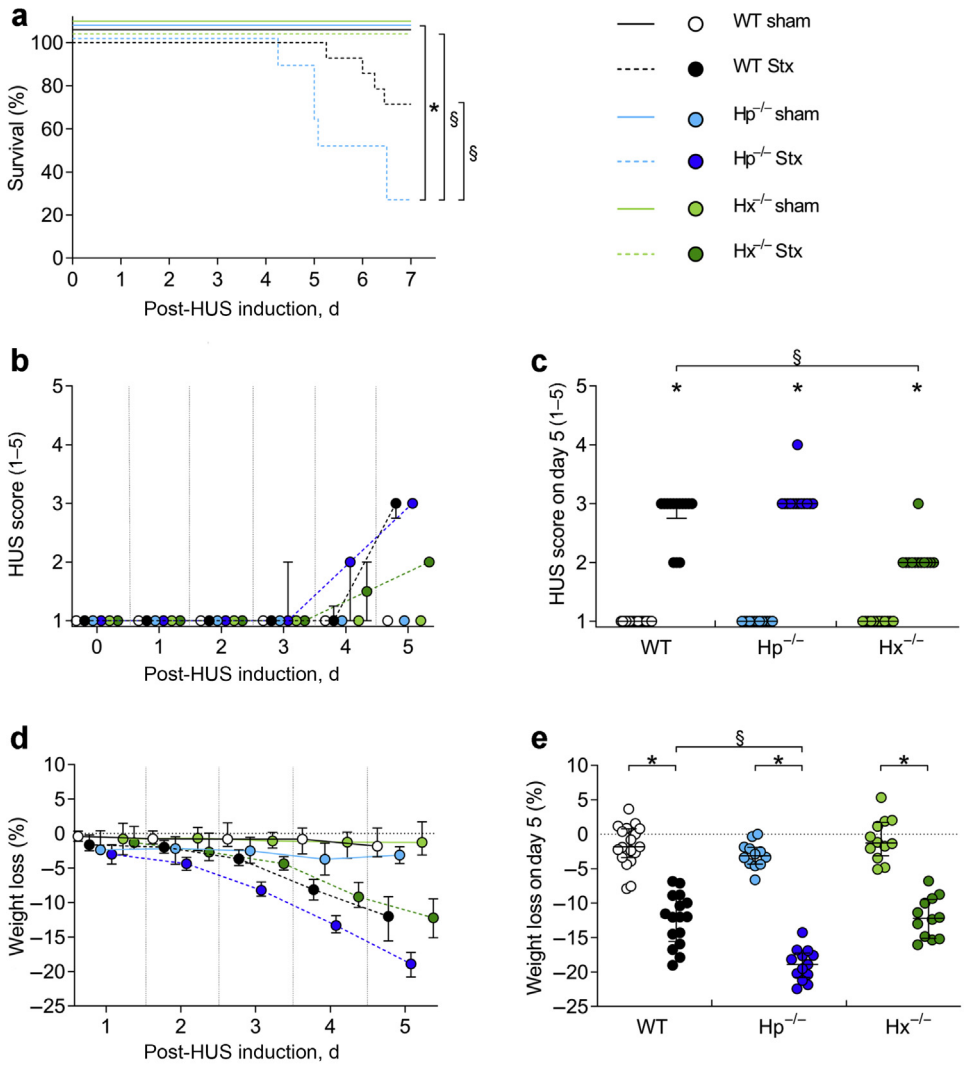

Figure 1 | Clinical presentation of wild-type (WT), haptoglobin$^{-/-}$ (Hp$^{-/-}$), and hemopexin$^{-/-}$ (Hx$^{-/-}$) mice with experimental hemolytic-uremic syndrome (HUS). (**a**) Kaplan-Meier survival analysis of sham mice and mice subjected to Shiga toxin (Stx; WT sham: $n = 9$; WT Stx: $n = 14$; Hp$^{-/-}$ sham: $n = 8$; Hp$^{-/-}$ Stx: $n = 8$; Hx$^{-/-}$ sham: $n = 8$; Hx$^{-/-}$ Stx: $n = 8$) in experimental HUS followed up for 7 days. *$P <$ 0.05 versus the corresponding sham group, §$P < 0.05$ versus the indicated Stx group (log-rank Mantel-Cox test). (**b–e**) Experimental HUS followed up for 5 days in sham mice and mice subjected to Stx (WT sham: $n = 19$; WT Stx: $n = 14$; Hp$^{-/-}$ sham: $n = 13$; Hp$^{-/-}$ Stx: $n = 13$; Hx$^{-/-}$ sham: $n = 12$; Hx$^{-/-}$ Stx: $n = 12$). (**b**) Evaluation of disease progression by HUS score (ranging from 1 = very active to 5 = dead) over 5 days. (**c**) Significant changes in HUS score on day 5 of sham mice and mice subjected to Stx. (**d**) Progression of weight loss from day 1 to day 5 in sham mice and mice subjected to Stx. (**e**) Significant changes in weight loss on day 5 in sham mice and mice subjected to Stx. Data are expressed as (**b,d**) dot plot, and (**c,e**) scatter dot plot with median (interquartile range) for n observations. *$P < 0.05$ versus the corresponding sham group, §$P < 0.05$ versus the WT Stx group (Mann-Whitney U test).

Renal endothelial cells are the main target of Stx by binding globotriaosylceramide receptors,[6] and apoptotic cells are increased in kidneys of patients with STEC-HUS.[37] A comparable loss of endothelial cells in all Stx-challenged genotypes indicated by CD31 expression (Figure 3e; Supplementary Figure S5B) and raised apoptosis indicated by CC-3 expression (Figure 3f; Supplementary Figure S5C) compared with their corresponding sham group was observed. Compared with Stx-challenged WT mice, Hx$^{-/-}$ mice expressed less CC-3.

Renal HO-1 expression was increased in Stx-challenged strains compared with their corresponding sham group (Figure 3g; Supplementary Figure S1A). Interestingly, HO-1 levels were the highest in Stx-challenged Hp$^{-/-}$ mice (15-fold), followed by WT mice (10-fold), whereas Hx$^{-/-}$ mice (6-fold) had the lowest levels.

Microthrombi formation in the kidneys is a hallmark of HUS pathology. Fibrin deposition was detected by acid fuchsin orange G staining in all Stx-challenged Hp$^{-/-}$ mice but only in some Stx-challenged WT and Hx$^{-/-}$ mice (Supplementary Figure S8).

Increased numbers of renal glycoprotein 1b–positive thrombocytes were observed in Stx-challenged WT and

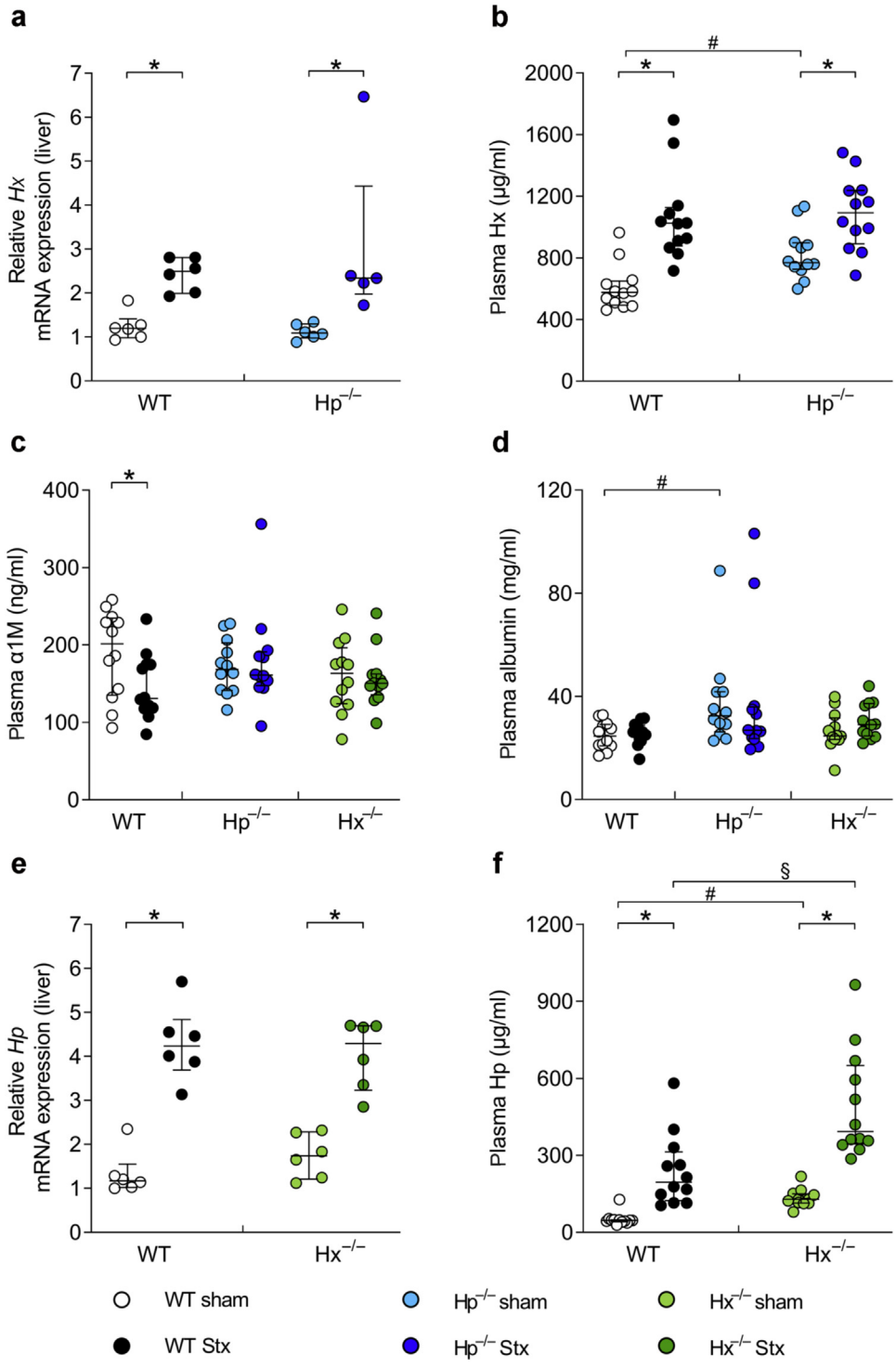

Figure 2 | Heme and haptoglobin (Hb) scavengers in wild-type (WT), haptoglobin$^{-/-}$ (Hp$^{-/-}$), and hemopexin$^{-/-}$ (Hx$^{-/-}$) mice with experimental hemolytic-uremic syndrome (HUS). (**a**) mRNA expression of *Hx* on day 5 in the liver of sham mice and mice subjected to Shiga toxin (Stx; $n = 6$ per group, except $n = 5$ for Hp$^{-/-}$ Stx). (**b**) Plasma Hx levels on day 5 of sham mice and mice subjected to Stx ($n = 12$ per group). Determination of plasma (**c**) α1-microglobulin (α1M) and (**d**) albumin levels on day 5 in sham mice and mice subjected to Stx ($n = 12$ per group). (**e**) mRNA expression of *Hp* on day 5 in the liver of sham mice and mice subjected to Stx ($n = 6$ per group). (**f**) Plasma Hp levels on day 5 of sham mice and mice subjected to Stx ($n = 12$ per group). (**a–f**) Data are expressed as scatter dot plot with median (interquartile range) for *n* observations. *$P < 0.05$ versus the corresponding sham group, #$P < 0.05$ versus the WT sham group, §$P < 0.05$ versus the WT Stx group (Mann-Whitney *U* test).

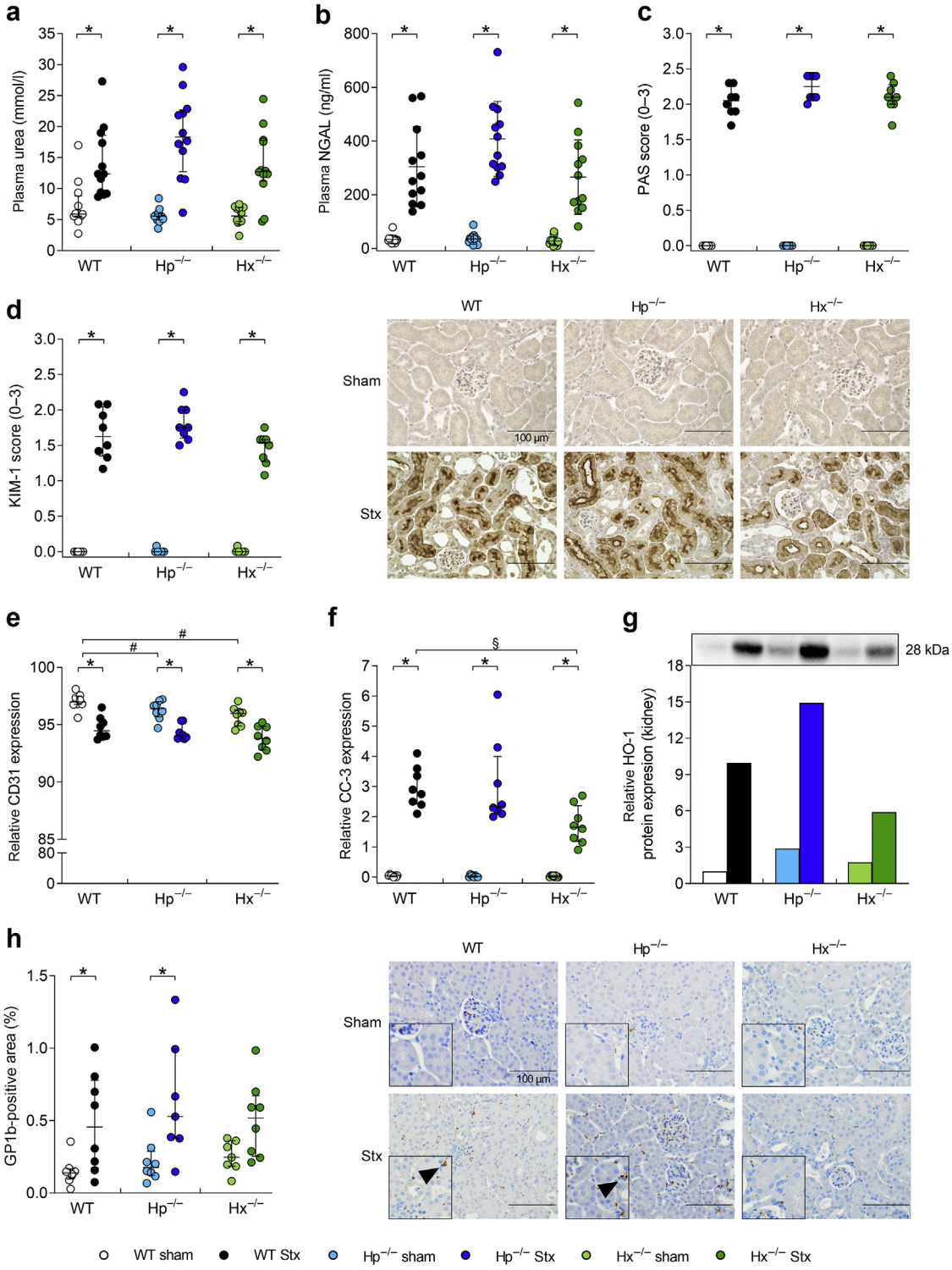

Figure 3 | Kidney injury and renal stress burden in wild-type (WT), haptoglobin$^{-/-}$ (Hp$^{-/-}$), and hemopexin$^{-/-}$ (Hx$^{-/-}$) mice with experimental hemolytic-uremic syndrome (HUS). Determination of (**a**) urea and (**b**) neutrophil gelatinase-associated lipocalin (NGAL) plasma levels on day 5 in sham mice and mice subjected to Shiga toxin (Stx; $n = 12$ per group). Quantification of (**c**) periodic acid–Schiff (PAS) reaction on day 5 in renal sections of sham mice and mice subjected to Stx ($n = 8$ per group). Quantification and representative pictures of immunohistochemical (**d**) kidney injury molecule-1 (KIM-1) staining on day 5 in renal sections of sham mice and mice subjected to Stx ($n = 8$ per group). Quantification of immunohistochemical (**e**) CD31 and (**f**) cleaved caspase-3 (CC-3) staining on day 5 in renal sections of sham mice and mice subjected to Stx ($n = 8$ per group). (**g**) Protein expression of heme oxygenase-1 (HO-1) on day 5 in the kidneys of sham mice and mice subjected to Stx. Samples from 6 animals per group were pooled to equal protein amounts for this representative blot ($n = 6$ per group). Individual blots (1 animal per group) are shown in Supplementary Figure S1A. (**h**) Quantification and representative pictures of immunohistochemical glycoprotein 1b (GP1b) staining on day 5 in renal sections of sham mice and (continued)

$Hp^{-/-}$ mice but not in $Hx^{-/-}$ mice compared with their corresponding sham group (Figure 3h).

Surrogate parameters of hemolysis in WT, $Hp^{-/-}$, and $Hx^{-/-}$ mice

An increased percentage of hemolysis and bilirubin plasma levels were detected in Stx-challenged WT and $Hp^{-/-}$ mice but not in $Hx^{-/-}$ mice compared with their corresponding sham group (Figure 4a and b). Hepatic and renal gene expression of proteins taking part in heme and iron homeostasis displayed varying regulations (Supplementary Figures S9 and S10). Hepatic *Hmox1* expression (Figure 4c) as well as levels of hepatic HO-1, Fth1, and CD163 were elevated in Stx-challenged WT mice but not in $Hp^{-/-}$ and $Hx^{-/-}$ mice compared with their corresponding sham group (Figure 4d–l).

Renal inflammation is attenuated in $Hx^{-/-}$ mice

Macrophage[37] and neutrophil[41] recruitment to the kidneys of patients with STEC-HUS has been described, and neutrophilia was shown to be associated with poor prognosis.[42,43] F4-80–positive macrophages were increased in the kidneys of Stx-challenged WT and $Hp^{-/-}$ mice but not in $Hx^{-/-}$ mice compared with their corresponding sham group (Figure 5a). F4-80 expression was elevated in $Hp^{-/-}$ sham mice compared with WT sham mice. Macrophages were decreased in Stx-challenged $Hp^{-/-}$ and $Hx^{-/-}$ mice compared with WT mice.

Lymphocyte antigen 6 complex, locus G expression, indicating neutrophil granulocyte recruitment, was elevated in the kidneys of Stx-challenged WT and $Hp^{-/-}$ mice but not in $Hx^{-/-}$ mice compared with their corresponding sham group (Figure 5b).

C3c deposition, indicating complement activation, was increased in all Stx-challenged mice compared with their corresponding sham group. C3c expression was elevated in Stx-challenged $Hp^{-/-}$ mice compared with WT mice (Figure 5c).

Hp intervention in WT mice

Stx-challenged WT mice received low-dose Hp, which has been reported to be beneficial in septic mice,[44] to evaluate its protective function in HUS-like disease (Figure 6a). Stx groups showed enhanced neutrophil gelatinase–associated lipocalin plasma levels, altered renal morphology, increased expression of kidney injury molecule-1, CC-3, and F4-80–positive macrophages, and C3c in the kidneys compared with their corresponding sham groups (Figure 6b–g). Renal glycoprotein 1b and lymphocyte antigen 6 complex, locus G expression was elevated in the Stx-challenged vehicle group but not in Hp-treated mice with HUS compared with the corresponding control group (Figure 6h and i). Hp-treated mice with HUS showed decreased lymphocyte antigen 6 complex, locus G expression compared with the corresponding vehicle group (Figure 6i).

Tubular iron deposition is increased in $Hp^{-/-}$ mice but not in WT and $Hx^{-/-}$ mice

Hp and Hx take part in iron homeostasis by their scavenging function regarding Hb and heme-bound iron. Pronounced iron deposition was detected in tubules of the $Hp^{-/-}$ strain but not in the WT and $Hx^{-/-}$ strains, irrespective of treatment (Figure 7a). Iron-positive tubules were increased in Stx-challenged $Hp^{-/-}$ mice compared with their corresponding sham group. Accordingly, highest renal Fth1 expression was found in $Hp^{-/-}$, followed by $Hx^{-/-}$ mice, whereas WT mice had the lowest levels (Figure 7b). Fth1 expression was slightly elevated in all Stx-challenged mice compared with their corresponding sham group.

We analyzed divalent metal transporter 1 and megalin and cubilin that are responsible for the cellular uptake of iron[45] and Hb,[46] respectively. Divalent metal transporter 1 expression was reduced in Stx-challenged $Hx^{-/-}$ mice but not in WT and $Hp^{-/-}$ mice compared with their corresponding sham group (Supplementary Figure S11A). Megalin and cubilin expression was high in all genotypes independent of Stx challenge (Supplementary Figure S11B and C).

Hepcidin plasma levels were increased in all Stx-challenged mice compared with their corresponding sham group (Figure 7c). Hepcidin plasma levels were elevated in Stx-challenged $Hp^{-/-}$ mice compared with WT Stx mice. Ferroportin-positive tubules were decreased in all Stx-challenged genotypes compared with their corresponding sham group (Figure 7d), in Stx-challenged $Hp^{-/-}$ mice compared with WT mice, and in $Hp^{-/-}$ sham mice compared with WT sham mice.

Renal malondialdehyde, nitrotyrosine, and nicotinamide adenine dinucleotide phosphate oxidase 1 were investigated as markers for oxidative stress. Malondialdehyde was enhanced in $Hp^{-/-}$ mice compared with WT mice, independent of Stx challenge. Nitrotyrosine and nicotinamide adenine dinucleotide phosphate oxidase 1 expression were increased in Stx-challenged $Hp^{-/-}$ mice compared with WT mice (Supplementary Figure S12).

DISCUSSION

We showed that Hp and Hx deficiency play divergent roles in disease progression in HUS, indicated by a survival advantage of $Hx^{-/-}$ mice and a higher mortality rate in $Hp^{-/-}$ mice compared with WT mice. Albeit the role of Hx in infectious diseases is discussed controversially, we hypothesized that both scavenger proteins are required for the resolution of HUS pathology accompanied by hemolysis. Thus, the survival

Figure 3 | (continued) mice subjected to Stx ($n = 8$ per group). Arrowheads indicate positive areas. Bar = 100 μm. Data are expressed as (**a–f,h**) scatter dot plot with median (interquartile range) for *n* observations and (**g**) bar graph. *$P < 0.05$ versus the corresponding sham group, #$P < 0.05$ versus the WT sham group, §$P < 0.05$ versus the WT Stx group (Mann-Whitney *U*-test). To optimize viewing of this image, please see the online version of this article at www.kidney-international.org.

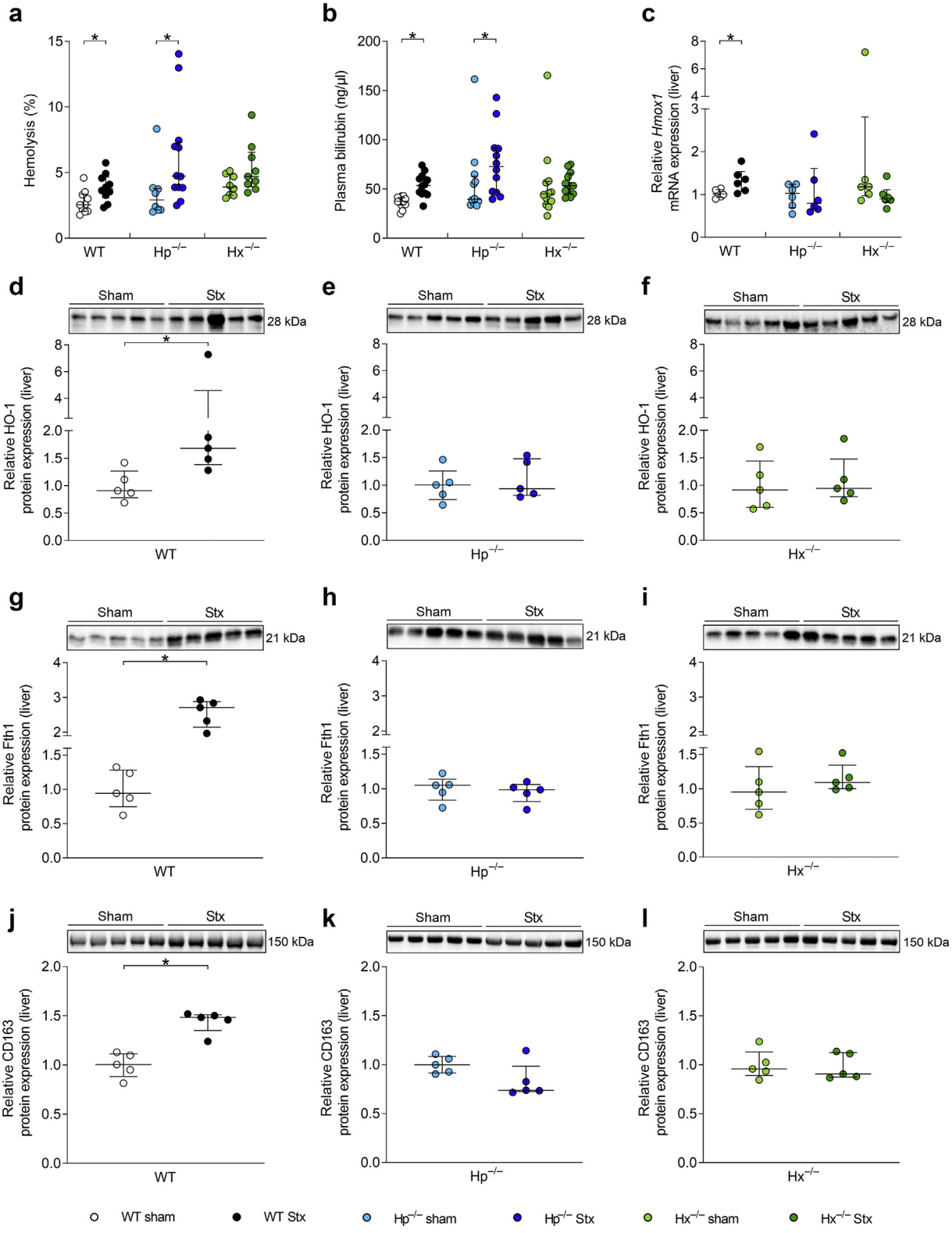

Figure 4 | Hemolysis in wild-type (WT), haptoglobin$^{-/-}$ (Hp$^{-/-}$), and hemopexin$^{-/-}$ (Hx$^{-/-}$) mice with experimental hemolytic-uremic syndrome (HUS). Determination of (**a**) percentage of hemolysis and (**b**) bilirubin plasma levels on day 5 in sham mice and mice subjected to Shiga toxin (Stx; hemolysis: WT sham: $n = 10$; WT Stx: $n = 10$; Hp$^{-/-}$ sham: $n = 8$; Hp$^{-/-}$ Stx: $n = 7$; Hx$^{-/-}$ sham: $n = 8$, Hx$^{-/-}$ Stx: $n = 9$; bilirubin: $n = 12$ per group). (**c**) mRNA expression of *Hmox1* (heme oxygenase-1) on day 5 in the liver of sham mice and mice subjected to Stx ($n = 6$ per group). Protein expression of heme oxygenase-1 (HO-1) on day 5 in the liver of (**d**) WT, (**e**) Hp$^{-/-}$, and (**f**) Hx$^{-/-}$ sham mice and mice subjected to Stx ($n = 5$ per group). Protein expression of ferritin heavy chain (Fth1) on day 5 in the liver of (**g**) WT, (continued)

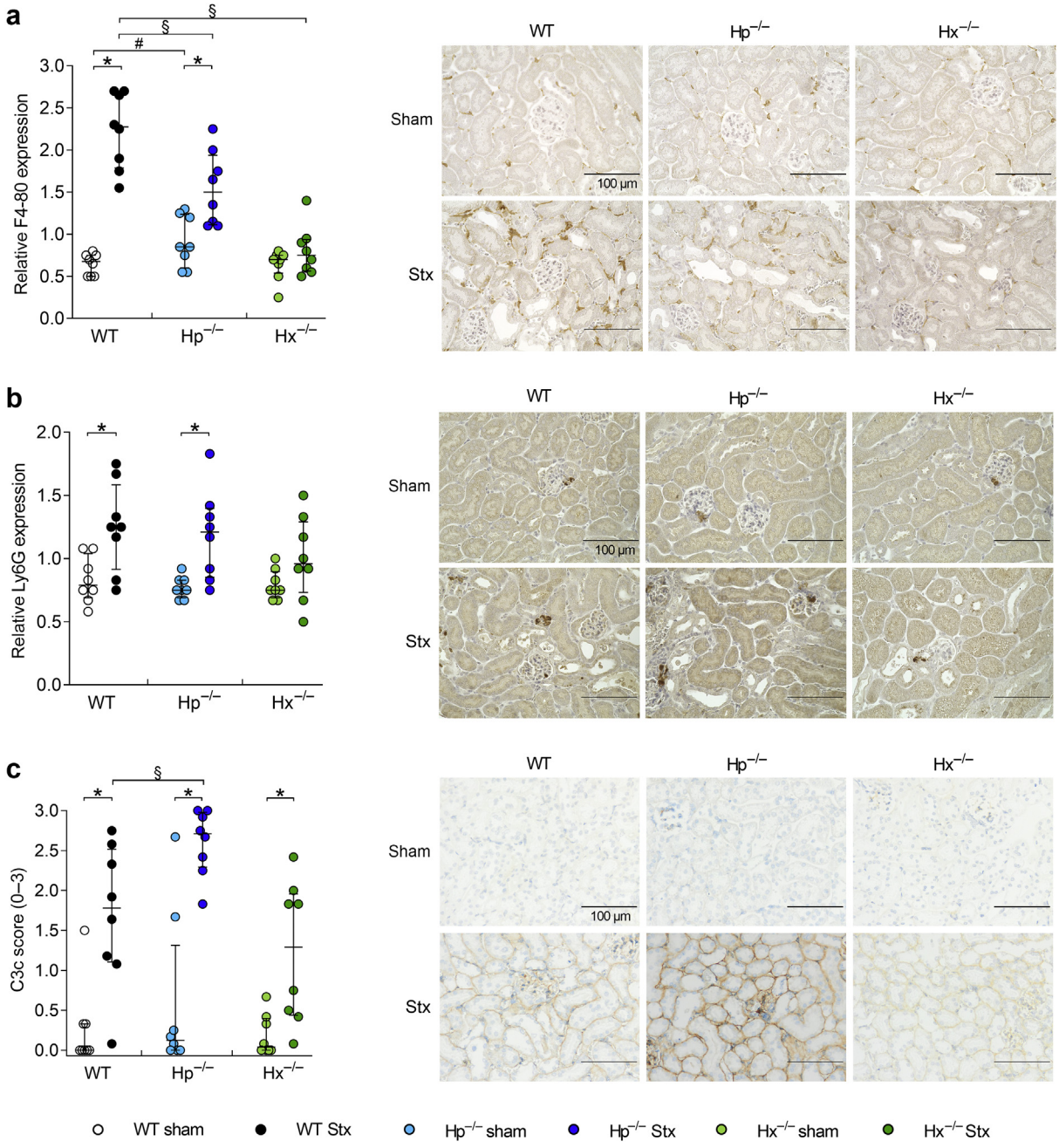

Figure 5 | Immune response in wild-type (WT), haptoglobin$^{-/-}$ (Hp$^{-/-}$), and hemopexin$^{-/-}$ (Hx$^{-/-}$) mice with experimental hemolytic-uremic syndrome (HUS). Quantification and representative pictures of immunohistochemical (**a**) F4-80, (**b**) lymphocyte antigen 6 complex, locus G (Ly6G), and (**c**) complement component 3 (C3c) staining on day 5 in renal sections of sham mice and mice subjected to Shiga toxin (Stx; $n = 8$ per group). Bar = 100 µm. (**a–c**) Data are expressed as scatter dot plot with median (interquartile range) for n observations. *$P < 0.05$ versus the corresponding sham group, #$P < 0.05$ versus the WT sham group, §$P < 0.05$ versus the WT Stx group (Mann-Whitney U test). To optimize viewing of this image, please see the online version of this article at www.kidney-international.org.

benefit of Hx$^{-/-}$ mice appeared unexpected to us, in particular, as Hx administration has been described to be protective in a murine model of sepsis, with a moderate degree of hemolysis[8] as well as in a model of sickle cell disease, with severe hemolysis.[7] However, in line with our results, Spiller *et al.* showed that Hx deficiency was protective in septic

Figure 4 | (continued) (**h**) Hp$^{-/-}$, and (**i**) Hx$^{-/-}$ sham mice and mice subjected to Stx ($n = 5$ per group). Protein expression of CD163 on day 5 in the liver of (**j**) WT, (**k**) Hp$^{-/-}$, and (**l**) Hx$^{-/-}$ sham mice and mice subjected to Stx ($n = 5$ per group). (**a–l**) Data are expressed as scatter dot plot with median (interquartile range) for n observations. *$P < 0.05$ versus the corresponding sham group. To optimize viewing of this image, please see the online version of this article at www.kidney-international.org.

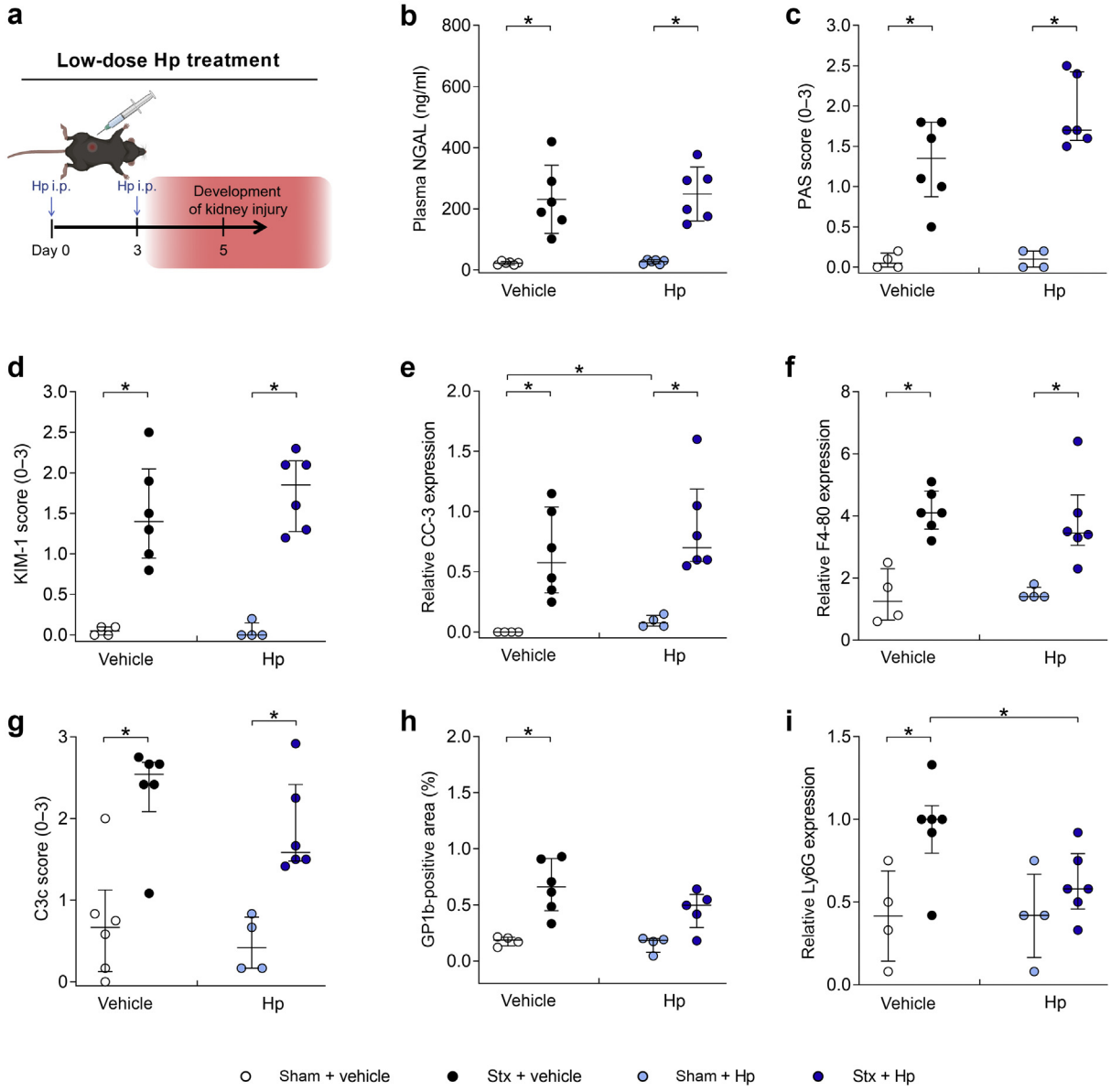

Figure 6 | Effect of haptoglobin (Hp) treatment on kidney injury and inflammation in wild-type (WT) mice with experimental hemolytic-uremic syndrome (HUS). (**a**) Application regime for low-dose Hp treatment of sham mice and mice subjected to Shiga toxin (Stx). (**b**) Determination of neutrophil gelatinase-associated lipocalin (NGAL) plasma levels on day 5 in sham mice and mice subjected to Stx, which were treated with Hp or vehicle ($n = 6$ per treatment group). Quantification of (**c**) periodic acid–Schiff (PAS) reaction, immunohistochemical (**d**) kidney injury molecule-1 (KIM-1), (**e**) cleaved caspase-3 (CC-3), (**f**) F4-80, (**g**) complement component 3 (C3c), (**h**) glycoprotein 1b (GP1b), and (**i**) lymphocyte antigen 6 complex, locus G (Ly6G) staining on day 5 in renal sections of sham mice and mice subjected to Stx, which were treated with Hp or vehicle (sham + vehicle, sham + Hp: $n = 4$ per group; Stx + vehicle, Stx + Hp: $n = 6$ per group; GP1b: Stx + Hp: $n = 5$ per group). (**c–i**) Data are expressed as scatter dot plot with median (interquartile range) for n observations. *$P < 0.05$ versus the corresponding sham group (Mann-Whitney U test).

mice.[47] The high mortality rate of $Hp^{-/-}$ mice with HUS was consistent with previously reported aggravated vulnerability under hemolytic,[29] inflammatory,[48] and septic[44] conditions and emphasizes the physiological relevance of Hp in diseases accompanied by hemolysis.

To evaluate possible mechanisms underlying the observed outcome of mice with HUS, we assessed various organ systems, such as kidneys, liver, lung, and colon, for pathological changes. We found obvious morphological alterations only in the kidneys of Stx-challenged mice.

Acute TMA-derived hemolysis is a disease-defining feature in patients with STEC-HUS.[49] Fibrin deposition in the kidneys was present in some $Hx^{-/-}$ and WT mice with HUS. However, unlike in Stx-challenged WT mice, platelet deposition in the kidneys as a surrogate parameter of TMA was not significantly increased in Stx-challenged $Hx^{-/-}$ mice

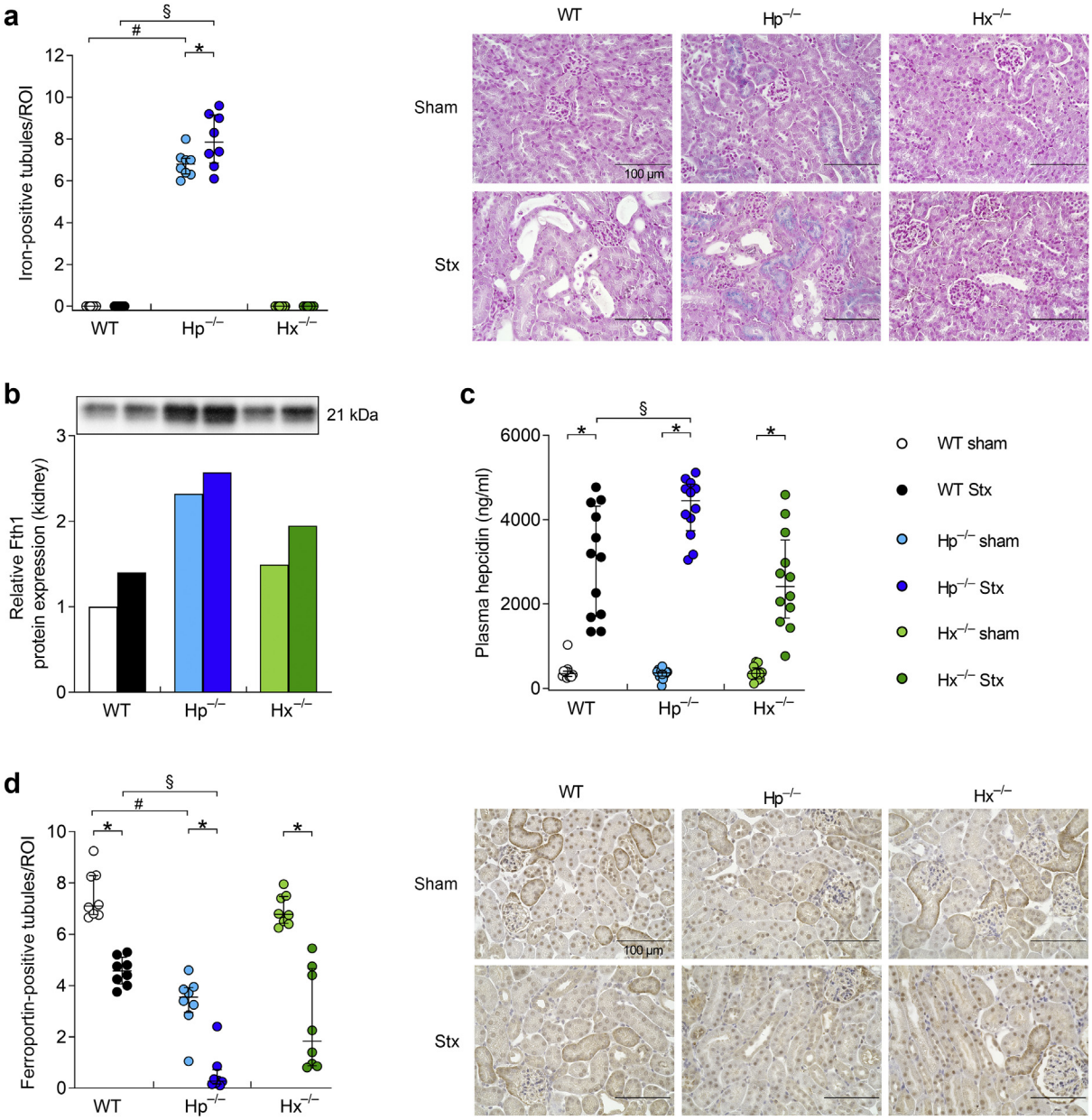

Figure 7 | Renal iron homeostasis in wild-type (WT), haptoglobin$^{-/-}$ (Hp$^{-/-}$), and hemopexin$^{-/-}$ (Hx$^{-/-}$) mice with experimental hemolytic-uremic syndrome (HUS). (**a**) Quantification and representative pictures of iron staining on day 5 in renal sections of sham mice and mice subjected to Shiga toxin (Stx; $n = 8$ per group). (**b**) Protein expression of ferritin heavy chain (Fth1) on day 5 in the kidneys of sham mice and mice subjected to Stx. Samples from 6 animals per group were pooled to equal protein amounts for this representative blot ($n = 6$ per group). Individual blots (1 animal per group) are shown in Supplementary Figure S1B. (**c**) Hepcidin plasma levels on day 5 of sham mice and mice subjected to Stx ($n = 6$ per group). Quantification and representative pictures of immunohistochemical (**d**) ferroportin staining on day 5 in renal sections of sham mice and mice subjected to Stx ($n = 8$ per group). Bar = 100 µm. Data are expressed as (**a,c,d**) scatter dot plot and (**b**) bar graph with median (interquartile range) for *n* observations. *$P < 0.05$ versus the corresponding sham group, #$P < 0.05$ versus the WT sham group, §$P < 0.05$ versus the WT Stx group (Mann-Whitney *U* test). ROI, region of interest. To optimize viewing of this image, please see the online version of this article at www.kidney-international.org.

compared with their corresponding sham group. These findings indicate attenuated TMA in Stx-challenged Hx$^{-/-}$ mice. Furthermore, apoptosis and HO-1 expression in the kidneys, as surrogate parameters for inflammation,[50] hypoxia,[51] and accumulation of heme,[52] were less pronounced in Hx$^{-/-}$ mice than in WT mice with HUS. In line with this, we found moderate hemolysis and increased bilirubin levels in WT mice but not in Hx$^{-/-}$ mice with HUS. Consequently, we observed an induction of hepatic HO-1, Fth1, and CD163 in Stx-challenged WT mice but not in Hx$^{-/-}$ mice, most likely indicating the clearance of Hp-Hb complexes by liver macrophages via CD163.[15,53] Of note, in patients with HUS, high plasma heme levels have been reported to be associated with high plasma HO-1 levels.[12]

It has been reported that Stx- and heme-mediated cytotoxicity is sensitized by inflammation.[54,55] Furthermore, macrophage[37] and neutrophil recruitment[41] to the kidneys are observed in renal biopsies of patients with STEC-HUS. In Stx-challenged $Hx^{-/-}$ mice, renal inflammation was less pronounced. This was indicated by reduced macrophage expression compared to Stx-challenged WT mice and by attenuated neutrophil expression. Considering our results, we conclude that Hx deficiency improves the survival of mice with HUS by ameliorating renal pathology and consequently reducing fatal events resulting from end-stage kidney disease.

$Hx^{-/-}$ mice with or without artificial hemolysis have been described to display higher endogenous Hp levels.[35] We could reproduce this finding in $Hx^{-/-}$ mice with or without HUS. Unlike patients with STEC-HUS, who often display depleted Hp levels[12] most likely as a sign of plasma Hp consumption, the acute phase reaction with high Hp expression seems to predominate in mice with HUS. Various anti-inflammatory and immunomodulatory functions of Hp have been reported, such as inhibiting calcium influx and subsequent oxidative burst by binding to activated neutrophils[56] and suppressing lipopolysaccharide-induced tumor necrosis factor-α production of macrophages.[48] Therefore, we hypothesized that increased Hp plasma levels in $Hx^{-/-}$ mice compared with WT mice might contribute to the protective effects of the constitutional Hx knockout. Treatment of Stx-challenged WT mice with low-dose Hp attenuated renal platelet deposition and neutrophil recruitment. Interestingly, it has been shown recently that reduction of neutrophil recruitment to the kidneys of WT mice with HUS by inhibition of CXC chemokine receptor 2 conveys renal protection.[57] However, as low-dose Hp administration did not attenuate kidney injury and CC-3 expression, our results indicate that elevated endogenous Hp expression in $Hx^{-/-}$ mice alone does not explain all beneficial effects observed in these mice.

We further investigated the effect of Hp deficiency on renal pathology. We identified similar patterns of tubular damage and thrombocyte depositions in the kidneys of $Hp^{-/-}$ and WT mice with HUS. This is consistent with the findings of Fagoonee *et al.*, showing no differences in kidney injury between $Hp^{-/-}$ and WT mice subjected to ischemia/reperfusion injury.[46] But fibrin deposition indicating microthrombi formation, a surrogate parameter for TMA, was increased in the kidneys of Stx-challenged $Hp^{-/-}$ mice compared with WT mice.

Interestingly, Hx plasma levels were higher in $Hp^{-/-}$ sham mice than in WT sham mice, suggesting a compensatory adaptation of the Hp-deficient genotype. After Stx challenge, plasma Hx levels increased in WT mice and even further in $Hp^{-/-}$ mice, suggesting that, similar to Hp, rather than the Hx consumption the acute phase reaction prevails in mice with HUS. However, in patients with STEC-HUS and hemolysis, Hx depletion has been reported.[12] There is first evidence that Hx can cause a nephrin-dependent remodeling of the actin cytoskeleton in podocytes,[58] which is supported by the observation that unilateral renal infusion of rats with Hx leads to glomerular alterations with concomitant proteinuria.[59,60] In our studies, we detected no ultrastructural changes in podocytes independent of genotype or intervention. Assumedly, the increase in Hx reflects a compensatory mechanism to detoxify heme in the absence of Hp and/or in Stx-induced HUS-like disease with a moderate degree of hemolysis.

We observed a disturbed iron homeostasis, elevated markers of oxidative stress, and increased complement activation in the kidneys of Stx-challenged $Hp^{-/-}$ mice compared with WT mice, which might explain the detrimental survival of $Hp^{-/-}$ mice with HUS.

Specifically, we found not only elevated plasma hepcidin levels and decreased ferroportin-positive tubuli in Stx-challenged $Hp^{-/-}$ mice compared with WT mice but also tubular iron deposition in $Hp^{-/-}$ sham mice, which further increased after Stx challenge. In line with this observation, a strong enhancement of Hb-derived iron in tubules of adult $Hp^{-/-}$ sham mice has been described to accumulate with age and after ischemia/reperfusion injury.[46] Other studies showed nephrotoxic effects in experimental hemochromatosis[61] or chronic hemosiderosis[62] in rats. Thus, the observed iron deposition is likely to contribute to the detrimental outcome of Stx-challenged $Hp^{-/-}$ mice. To date, there are no studies examining iron homeostasis in patients with STEC-HUS. However, a study analyzing genetic polymorphisms in patients with STEC-HUS suggests that genes encoding for proteins involved in iron transport might influence the host susceptibility to develop HUS.[63] There is increasing evidence that in the absence of Hp, Hb is glomerular filtered and that the tubular uptake through megalin and cubilin prevents urinary iron loss.[17,64] We observed elevated renal HO-1 expression and acute tubular iron deposition in Stx-challenged $Hp^{-/-}$ mice, indicating alterations in renal heme and iron homeostasis. Unlike in WT mice, we found no induction of hepatic HO-1, Fth1, and CD163 in Stx-challenged $Hp^{-/-}$ mice, suggesting that Hb cannot be cleared by liver macrophages via CD163 because of Hp deficiency. In hemolytic disease, it has been shown that liver macrophages can switch to a proinflammatory phenotype in the presence of heme and iron.[7] In this study, we did not characterize the macrophage phenotype. However, quantitatively, macrophage recruitment to the kidneys was surprisingly attenuated in Stx-challenged $Hp^{-/-}$ mice compared with WT mice.

Furthermore, markers of oxidative stress were elevated in Stx-challenged $Hp^{-/-}$ mice compared with WT mice. This finding might result from the observed tubular iron increase, as it has been described that heme-bound iron is a potent mediator for reactive oxygen species generation, which can lead to ferroptosis[65] and has been associated with thrombocyte activation *in vitro*.[66] In patients with HUS, enhanced lipid oxidation as a marker for oxidative stress has been shown to be increased and linked to hemolysis.[67]

There is evidence that complement activation occurs in the presence of heme in models of artificial hemolysis[10] and sickle cell disease.[9] Increased complement activation in the plasma of

patients with STEC-HUS has been described,[68] and preclinical studies suggest that this activation might lead to an aggravation of HUS pathology.[69–71] Accordingly, we found elevated C3c deposition in the kidneys of $Hp^{-/-}$ mice compared with WT mice with HUS.

We conclude that Hp and Hx deficiency plays divergent roles in HUS disease progression in mice. Although Stx-challenged $Hx^{-/-}$ mice were characterized by less disease severity and attenuated renal pathology, $Hp^{-/-}$ mice displayed a higher mortality rate, accompanied by iron and complement deposition in the kidneys. Low-dose Hp treatment of Stx-challenged WT mice attenuated surrogate parameters of renal TMA and inflammation, but not kidney injury. Thus, we suggest that Hp-dependent mechanisms convey—at least in part—protection and that Hp is important for the resolution of STEC-HUS pathology.

DISCLOSURE

All the authors declared no competing interests.

DATA STATEMENT

For original data, please contact sina.coldewey@med.uni-jena.de.

ACKNOWLEDGMENTS

We thank Jacqueline Fischer (Translational Septomics, Jena University Hospital, Jena, Germany) for technical assistance and Miguel Soares (Insitituto Gulbenkian de Ciência, Oeiras, Portugal) for providing us the breeding pairs of the knockout strains. We thank Michael Kiehntopf and Cora Richert (Department of Clinical Chemistry and Laboratory Medicine, Jena University Hospital) for the measurement of creatine, potassium, and alanine aminotransferase plasma levels. Mouse symbols were created with BioRender. The research leading to these results has received funding from the German Research Foundation (DFG, Research Unit FOR1738, award no. CO912/2-1 to SMC, award no. BA1601/8-2 to MB, and award no. HE2993/12-2 to SHH) and the Federal Ministry of Education and Research (BMBF, ZIK Septomics Research Center, Translational Septomics, award no. 03Z22JN12 to SMC).

AUTHOR CONTRIBUTIONS

SMC designed, planned, and supervised the study. SMC, WP, and ANM wrote the manuscript and revisions. WP and BW performed animal experiments with wild-type, haptoglobin$^{-/-}$, and hemopexin$^{-/-}$ mice, including data analysis. SK, BW, and NK performed animal experiments with haptoglobin administration, including data analysis. WP and ANM analyzed enzyme-linked immunosorbent assay data. WP, SK, and ANM performed histology and immunohistochemistry including data analysis. ANM performed gene expression, Western blot analyses, and hemolysis assay including data analysis. FG provided Shiga toxin. CD and KA planned and supervised histology of the liver, lung, and colon, immunohistochemistry for glycoprotein 1b, and electron microscopy and analyzed the corresponding data. SMC, WP, ANM, BW, NK, SK, CD, FG, ET, MB, KA, and SHH provided important intellectual content and revised the manuscript. All authors carefully reviewed and approved the manuscript.

SUPPLEMENTARY MATERIAL

Supplementary File (PDF)

Supplementary Methods.

Table S1. Hemolytic-uremic syndrome (HUS) score.

Table S2. Commercial kits.

Table S3. Primary antibodies used for immunohistochemistry.

Table S4. Secondary antibodies used for immunohistochemistry.

Table S5. PrimePCR assays (Bio-Rad Laboratories, Inc.) used for quantitative real-time polymerase chain reaction (PCR).

Table S6. Primary and secondary antibodies used for Western blot analyses.

Supplementary Results.

Figure S1. Renal protein expression of heme oxygenase-1 (HO-1) and ferritin heavy chain (Fth1) in wild-type (WT), haptoglobin (Hp)$^{-/-}$, and hemopexin (Hx)$^{-/-}$ mice with experimental hemolytic-uremic syndrome (HUS). Protein expression on day 5 of (**A**) HO-1 (28 kDa) and (**B**) Fth1 (21 kDa) in kidneys of sham mice and mice subjected to Shiga toxin (Stx). Each line represents a single blot of indicated strains and groups. Representative blots of pooled samples are shown in Figure 3g (HO-1) and Figure 7b (Fth1).

Figure S2. Granulomatous alterations in the liver of wild-type (WT), haptoglobin (Hp)$^{-/-}$, and hemopexin (Hx)$^{-/-}$ mice with experimental hemolytic-uremic syndrome (HUS). Quantification and representative pictures of hematoxylin and eosin (H&E) staining in liver sections on day 5 of sham mice and mice subjected to Shiga toxin (Stx; $n = 6$ per group). Bars = 500 μm. Data are expressed as scatter dot plot with median (interquartile range) for n observations. $^{*}P < 0.05$ versus the corresponding sham group, $^{\#}P < 0.05$ versus the WT sham group (Mann-Whitney U test).

Figure S3. Inflammatory alterations in lung and colon of wild-type (WT), haptoglobin (Hp)$^{-/-}$, and hemopexin (Hx)$^{-/-}$ mice with experimental hemolytic-uremic syndrome (HUS). Representative pictures of (**A**) periodic acid–Schiff (PAS) reaction in the lungs and (**B**) hematoxylin and eosin (H&E) staining in colon sections on day 5 of sham mice and mice subjected to Shiga toxin (Stx; $n = 6$ per group). (**A**) Bars = 200 μm. (**B**) Bars = 500 μm. Since no morphological changes were observed in the intestine and lung, only the presence of inflammatory cell aggregates was determined for these 2 organs (0 = absent; 1 = present). Few inflammatory cell aggregates were observed in the lung of WT sham (1/6), WT Stx (3/6), $Hp^{-/-}$ sham (2/6), $Hp^{-/-}$ Stx (2/6), $Hx^{-/-}$ sham (3/6), and $Hx^{-/-}$ Stx (3/6) mice. Few inflammatory cell aggregates were observed in the colon of WT sham (2/6), WT Stx (1/6), $Hp^{-/-}$ sham (4/6), $Hp^{-/-}$ Stx (3/6), $Hx^{-/-}$ sham (0/6), and $Hx^{-/-}$ Stx (2/6) mice.

Figure S4. Plasma levels of alanine aminotransferase (ALAT) and aspartate aminotransferase (ASAT) in wild-type (WT), haptoglobin (Hp)$^{-/-}$, and hemopexin (Hx)$^{-/-}$ mice with experimental hemolytic-uremic syndrome (HUS). Determination of (**A**) ALAT (WT sham, $n = 12$; WT Shiga toxin (Stx), $Hp^{-/-}$ sham and Stx, $Hx^{-/-}$ Stx, $n = 6$, sham; $Hx^{-/-}$, $n = 5$) and (**B**) ASAT (WT sham: $n = 18$; WT Stx: $n = 16$; $Hp^{-/-}$ sham and Stx: $n = 13$; $Hx^{-/-}$ sham and Stx: $n = 12$) plasma levels in sham mice and mice subjected to Stx on day 5. (**A,B**) Data are expressed as scatter dot plot with median (interquartile range) for n observations. $^{*}P < 0.05$ versus the corresponding sham group, $^{\#}P < 0.05$ versus the WT sham group (Mann-Whitney U test).

Figure S5. Renal periodic acid–Schiff (PAS) reaction and CD31 and cleaved caspase-3 (CC-3) staining in wild-type (WT), haptoglobin (Hp)$^{-/-}$, and hemopexin (Hx)$^{-/-}$ mice with experimental hemolytic-uremic syndrome (HUS). Representative pictures on day 5 of the (**A**) PAS reaction, immunohistochemical and (**B**) CD31 and (**C**) CC-3 staining in renal sections of sham mice and mice subjected to Shiga toxin (Stx; $n = 8$ per group). Bars = 100 μm. (**A–C**) Quantifications are shown in Figure 3c (PAS), Figure 3e (CD31), and Figure 3f (CC-3).

Figure S6. Kidney dysfunction in wild-type (WT), haptoglobin (Hp)$^{-/-}$, and hemopexin (Hx)$^{-/-}$ mice with experimental hemolytic-uremic

syndrome (HUS). Determination of (**A**) creatinine (WT sham: n = 12; WT Stx [Shiga toxin]: n = 11; $Hp^{-/-}$ sham: n = 9; $Hp^{-/-}$ Stx: n = 7; $Hx^{-/-}$ sham: n = 7; $Hx^{-/-}$ Stx: n = 8) and (**B**) potassium (WT sham: n = 11; WT Stx: n = 8; $Hp^{-/-}$ sham and Stx: n = 7; $Hx^{-/-}$ sham and Stx: n = 4) plasma levels of sham mice and mice subjected to Stx. (**A,B**) Data are expressed as a scatter dot plot with median (interquartile range) for *n* observations. $^{*}P < 0.05$ versus the corresponding sham group, $^{\S}P < 0.05$ versus the WT Stx group (Mann-Whitney *U* test).

Figure S7. Electron microscopic analysis of kidney tissue from wild-type (WT), haptoglobin $(Hp)^{-/-}$, and hemopexin $(Hx)^{-/-}$ mice with experimental hemolytic-uremic syndrome (HUS). Representative ultrastructural images on day 5 of sham mice and mice subjected to Shiga toxin (Stx). After HUS induction, only occasional widening of the podocyte foot processes (FPs) and the slightly swollen endothelium (EC) were observed in all genotypes. The fenestration of the EC was not noticeably altered due to the Stx challenge. The glomerular basement membranes were neither widened nor injured and mesangial cells appeared normal (N = nucleus; P = podocyte; RBC = red blood cell). Bar = 1 μm.

Figure S8. Fibrin depositions in the kidneys of wild-type (WT), haptoglobin $(Hp)^{-/-}$, and hemopexin $(Hx)^{-/-}$ mice with experimental hemolytic-uremic syndrome (HUS). Quantifications and representative pictures of acid fuchsin orange G (SGOF) staining on day 5 in renal sections of sham mice and mice subjected to Shiga toxin (Stx; $n = 8$ per group). Arrows indicate microthrombi. Bars = 100 μm. Data are expressed as a scatter dot plot with median (interquartile range) for *n* observations. $^{*}P < 0.05$ versus the corresponding sham group, $^{\S}P < 0.05$ versus the WT Stx group (Mann-Whitney *U* test).

Figure S9. Hepatic heme and iron metabolism in wild-type (WT), haptoglobin $(Hp)^{-/-}$, and hemopexin $(Hx)^{-/-}$ mice with experimental hemolytic-uremic syndrome (HUS). mRNA expression of (**A**) *CD163*, (**B**) transferrin (*Trf*), (**C**) LDL-receptor related protein 1 (*Lrp1*), (**D**) ferritin heavy chain (*Fth1*), (**E**) ferritin light chain (*Ftl1*), (**F**) albumin (*Alb*), and (**G**) ferroportin (*SCL40A1*) in livers of sham mice and mice subjected to Shiga toxin (Stx; $n = 6$ per group). (**A–G**) Data are expressed as a scatter dot plot with median (interquartile range) for *n* observations. $^{*}P < 0.05$ versus the corresponding sham group, $^{\#}P < 0.05$ versus the WT sham group, $^{\S}P < 0.05$ versus the WT Stx group (Mann-Whitney *U* test).

Figure S10. Renal heme and iron metabolism in wild-type (WT), haptoglobin $(Hp)^{-/-}$, and hemopexin $(Hx)^{-/-}$ mice with experimental hemolytic-uremic syndrome (HUS). mRNA expression of (**A**) albumin (*Alb*), (**B**) transferrin (*Trf*), (**C**) ferroportin (*SCL40A1*), (**D**) LDL-receptor related protein 1 (*Lrp1*), (**E**) ferritin light chain (*Ftl1*), (**F**) ferritin heavy chain (*Fth1*), (**G**) LDL-receptor related protein 2 (*Lrp2*), (**H**) cubilin (*Cubn*), and (**I**) heme oxygenase-1 (*Hmox1*) on day 5 in kidneys of sham mice and mice subjected to Shiga toxin (Stx; $n = 6$ per group). (**A–I**) Data are expressed as a scatter dot plot with median (interquartile range) for *n* observations. $^{*}P < 0.05$ versus the corresponding sham group, $^{\#}P < 0.05$ versus the WT sham group, $^{\S}P < 0.05$ versus the WT Stx group (Mann-Whitney *U* test).

Figure S11. Renal expression of divalent metal transporter 1 (DMT1), megalin, and cubilin in wild-type (WT), haptoglobin $(Hp)^{-/-}$, and hemopexin $(Hx)^{-/-}$ mice with experimental hemolytic-uremic syndrome (HUS). Quantification and representative pictures of immunohistochemical (**A**) DMT1, (**B**) megalin, and (**C**) cubilin staining on day 5 in renal sections of sham mice and mice subjected to Shiga toxin (Stx; $n = 8$ per group). Bars = 100 μm. (**A–C**) Data are expressed as a scatter dot plot with median (interquartile range) for *n* observations. $^{*}P < 0.05$ versus the corresponding sham group, $^{\S}P < 0.05$ versus the WT Stx group (Mann-Whitney *U* test).

Figure S12. Oxidative stress in the kidneys of wild-type (WT), haptoglobin $(Hp)^{-/-}$, and hemopexin $(Hx)^{-/-}$ mice with experimental hemolytic-uremic syndrome (HUS). (**A**) Malondialdehyde (MDA) levels on day 5 in kidneys of sham mice and mice subjected to Shiga toxin (Stx; $n = 6$ per group). Quantification of immunohistochemical (**B**) nitrotyrosine and (**C**) NADPH oxidase 1 (NOX-1) staining on day 5 in renal sections of sham mice and mice subjected to Stx ($n = 8$ per group). Bars = 100 μm. (**A–C**) Data are expressed as a scatter dot plot with median (interquartile range) for *n* observations. $^{*}P < 0.05$ versus the corresponding sham group, $^{\#}P < 0.05$ versus the WT sham group, $^{\S}P < 0.05$ versus the WT Stx group (Mann-Whitney *U* test).

Supplementary References.

REFERENCES

1. Fakhouri F, Zuber J, Frémeaux-Bacchi V, Loirat C. Haemolytic uraemic syndrome. *Lancet*. 2017;390:681–696.
2. Karmali MA. Infection by Shiga toxin-producing *Escherichia coli*: an overview. *Mol Biotechnol*. 2004;26:117–122.
3. Riley LW, Remis RS, Helgerson SD, et al. Hemorrhagic colitis associated with a rare *Escherichia coli* serotype. *N Engl J Med*. 1983;308:681–685.
4. Frank C, Werber D, Cramer JP, et al. Epidemic profile of Shiga-toxin-producing *Escherichia coli* O104:H4 outbreak in Germany. *N Engl J Med*. 2011;365:1771–1780.
5. Proulx F, Seidman EG, Karpman D. Pathogenesis of Shiga toxin-associated hemolytic uremic syndrome. *Pediatr Res*. 2001;50:163–171.
6. Mayer CL, Leibowitz CS, Kurosawa S, Stearns-Kurosawa DJ. Shiga toxins and the pathophysiology of hemolytic uremic syndrome in humans and animals. *Toxins (Basel)*. 2012;4:1261–1287.
7. Vinchi F, Costa da Silva M, Ingoglia G, et al. Hemopexin therapy reverts heme-induced proinflammatory phenotypic switching of macrophages in a mouse model of sickle cell disease. *Blood*. 2016;127:473–486.
8. Larsen R, Gozzelino R, Jeney V, et al. A central role for free heme in the pathogenesis of severe sepsis. *Sci Transl Med*. 2010;2:51ra71.
9. Merle NS, Grunenwald A, Rajaratnam H, et al. Intravascular hemolysis activates complement via cell-free heme and heme-loaded microvesicles. *JCI Insight*. 2018;3:e96910.
10. Merle NS, Paule R, Leon J, et al. P-selectin drives complement attack on endothelium during intravascular hemolysis in TLR-4/heme-dependent manner. *Proc Natl Acad Sci U S A*. 2019;116:6280–6285.
11. Dutra FF, Bozza MT. Heme on innate immunity and inflammation. *Front Pharmacol*. 2014;5:115.
12. Wijnsma KL, Veissi ST, de Wijs S, et al. Heme as possible contributing factor in the evolvement of Shiga-toxin *Escherichia coli* induced hemolytic-uremic syndrome. *Front Immunol*. 2020;11:547406.
13. Wang Y, Kinzie E, Berger FG, et al. Haptoglobin, an inflammation-inducible plasma protein. *Redox Rep*. 2001;6:379–385.
14. Nielsen MJ, Moestrup SK. Receptor targeting of hemoglobin mediated by the haptoglobins: roles beyond heme scavenging. *Blood*. 2009;114:764–771.
15. Kristiansen M, Graversen JH, Jacobsen C, et al. Identification of the haemoglobin scavenger receptor. *Nature*. 2001;409:198–201.
16. Tolosano E, Hirsch E, Patrucco E, et al. Defective recovery and severe renal damage after acute hemolysis in hemopexin-deficient mice. *Blood*. 1999;94:3906–3914.
17. Gburek J, Verroust PJ, Willnow TE, et al. Megalin and cubilin are endocytic receptors involved in renal clearance of hemoglobin. *J Am Soc Nephrol*. 2002;13:423–430.
18. Smith A, McCulloh RJ. Hemopexin and haptoglobin: allies against heme toxicity from hemoglobin not contenders. *Front Physiol*. 2015;6:187.
19. Tolosano E, Cutufia MA, Hirsch E, et al. Specific expression in brain and liver driven by the hemopexin promoter in transgenic mice. *Biochem Biophys Res Commun*. 1996;218:694–703.
20. Paoli M, Anderson BF, Baker HM, et al. Crystal structure of hemopexin reveals a novel high-affinity heme site formed between two β-propeller domains. *Nat Struct Biol*. 1999;6:926–931.
21. Hvidberg V, Maniecki MB, Jacobsen C, et al. Identification of the receptor scavenging hemopexin-heme complexes. *Blood*. 2005;106:2572–2579.
22. Ryter SW, Alam J, Choi AM. Heme oxygenase-1/carbon monoxide: from basic science to therapeutic applications. *Physiol Rev*. 2006;86:583–650.
23. Bitzan M, Bickford BB, Foster GH. Verotoxin (Shiga toxin) sensitizes renal epithelial cells to increased heme toxicity: possible implications for the hemolytic uremic syndrome. *J Am Soc Nephrol*. 2004;15:2334–2343.

24. Suttner DM, Dennery PA. Reversal of HO-1 related cytoprotection with increased expression is due to reactive iron. *FASEB J*. 1999;13:1800–1809.
25. Maines MD. The heme oxygenase system: a regulator of second messenger gases. *Annu Rev Pharmacol Toxicol*. 1997;37:517–554.
26. Epsztejn S, Glickstein H, Picard V, et al. H-ferritin subunit overexpression in erythroid cells reduces the oxidative stress response and induces multidrug resistance properties. *Blood*. 1999;94:3593–3603.
27. Lawson DM, Artymiuk PJ, Yewdall SJ, et al. Solving the structure of human H ferritin by genetically engineering intermolecular crystal contacts. *Nature*. 1991;349:541–544.
28. Hentze MW, Muckenthaler MU, Galy B, Camaschella C. Two to tango: regulation of mammalian iron metabolism. *Cell*. 2010;142:24–38.
29. Lim SK, Kim H, Lim SK, et al. Increased susceptibility in Hp knockout mice during acute hemolysis. *Blood*. 1998;92:1870–1877.
30. Dennhardt S, Pirschel W, Wissuwa B, et al. Modeling hemolytic-uremic syndrome: in-depth characterization of distinct murine models reflecting different features of human disease. *Front Immunol*. 2018;9:1459.
31. Sobbe IV, Krieg N, Dennhardt S, Coldewey SM. Involvement of NF-κB1 and the non-canonical NF-κB signaling pathway in the pathogenesis of acute kidney injury in Shiga-toxin-2-induced hemolytic-uremic syndrome in mice. *Shock*. 2021;56:573–581.
32. Pfaffl MW. A new mathematical model for relative quantification in real-time RT-PCR. *Nucleic Acids Res*. 2001;29:e45.
33. Rivero-Gutiérrez B, Anzola A, Martínez-Augustin O, de Medina FS. Stain-free detection as loading control alternative to Ponceau and housekeeping protein immunodetection in Western blotting. *Anal Biochem*. 2014;467:1–3.
34. Ofori-Acquah SF, Hazra R, Orikogbo OO, et al. Hemopexin deficiency promotes acute kidney injury in sickle cell disease. *Blood*. 2020;135:1044–1048.
35. Tolosano E, Fagoonee S, Hirsch E, et al. Enhanced splenomegaly and severe liver inflammation in haptoglobin/hemopexin double-null mice after acute hemolysis. *Blood*. 2002;100:4201–4208.
36. Ascenzi P, di Masi A, Fanali G, Fasano M. Heme-based catalytic properties of human serum albumin. *Cell Death Discov*. 2015;1:15025.
37. Porubsky S, Federico G, Müthing J, et al. Direct acute tubular damage contributes to Shigatoxin-mediated kidney failure. *J Pathol*. 2014;234:120–133.
38. Ozaki M, Kang Y, Tan YS, et al. Human mannose-binding lectin inhibitor prevents Shiga toxin-induced renal injury. *Kidney Int*. 2016;90:774–782.
39. Motto DG, Chauhan AK, Zhu G, et al. Shigatoxin triggers thrombotic thrombocytopenic purpura in genetically susceptible ADAMTS13-deficient mice. *J Clin Invest*. 2005;115:2752–2761.
40. Keepers TR, Psotka MA, Gross LK, Obrig TG. A murine model of HUS: Shiga toxin with lipopolysaccharide mimics the renal damage and physiologic response of human disease. *J Am Soc Nephrol*. 2006;17:3404–3414.
41. Inward CD, Howie AJ, Fitzpatrick MM, et al. British Association for Paediatric Nephrology. Renal histopathology in fatal cases of diarrhoea-associated haemolytic uraemic syndrome. *Pediatr Nephrol*. 1997;11:556–559.
42. Walters MD, Matthei IU, Kay R, et al. The polymorphonuclear leucocyte count in childhood haemolytic uraemic syndrome. *Pediatr Nephrol*. 1989;3:130–134.
43. Fernandez GC, Gomez SA, Ramos MV, et al. The functional state of neutrophils correlates with the severity of renal dysfunction in children with hemolytic uremic syndrome. *Pediatr Res*. 2007;61:123–128.
44. Yang H, Wang H, Levine YA, et al. Identification of CD163 as an antiinflammatory receptor for HMGB1-haptoglobin complexes. *JCI Insight*. 2016;1:e85375.
45. Moulouel B, Houamel D, Delaby C, et al. Hepcidin regulates intrarenal iron handling at the distal nephron. *Kidney Int*. 2013;84:756–766.
46. Fagoonee S, Gburek J, Hirsch E, et al. Plasma protein haptoglobin modulates renal iron loading. *Am J Pathol*. 2005;166:973–983.
47. Spiller F, Costa C, Souto FO, et al. Inhibition of neutrophil migration by hemopexin leads to increased mortality due to sepsis in mice. *Am J Respir Crit Care Med*. 2011;183:922–931.
48. Arredouani MS, Kasran A, Vanoirbeek JA, et al. Haptoglobin dampens endotoxin-induced inflammatory effects both in vitro and in vivo. *Immunology*. 2005;114:263–271.
49. Argyle JC, Hogg RJ, Pysher TJ, et al. A clinicopathological study of 24 children with hemolytic uremic syndrome: a report of the Southwest Pediatric Nephrology Study Group. *Pediatr Nephrol*. 1990;4:52–58.
50. Vogt BA, Shanley TP, Croatt A, et al. Glomerular inflammation induces resistance to tubular injury in the rat: a novel form of acquired, heme oxygenase-dependent resistance to renal injury. *J Clin Invest*. 1996;98:2139–2145.
51. Shimizu H, Takahashi T, Suzuki T, et al. Protective effect of heme oxygenase induction in ischemic acute renal failure. *Crit Care Med*. 2000;28:809–817.
52. Nath KA, Balla G, Vercellotti GM, et al. Induction of heme oxygenase is a rapid, protective response in rhabdomyolysis in the rat. *J Clin Invest*. 1992;90:267–270.
53. Theurl I, Hilgendorf I, Nairz M, et al. On-demand erythrocyte disposal and iron recycling requires transient macrophages in the liver. *Nat Med*. 2016;22:945–951.
54. Seixas E, Gozzelino R, Chora A, et al. Heme oxygenase-1 affords protection against noncerebral forms of severe malaria. *Proc Natl Acad Sci U S A*. 2009;106:15837–15842.
55. van Setten PA, van Hinsbergh VW, van der Velden TJ, et al. Effects of TNFα on verocytotoxin cytotoxicity in purified human glomerular microvascular endothelial cells. *Kidney Int*. 1997;51:1245–1256.
56. Oh SK, Pavlotsky N, Tauber AI. Specific binding of haptoglobin to human neutrophils and its functional consequences. *J Leukoc Biol*. 1990;47:142–148.
57. Lill JK, Thiebes S, Pohl JM, et al. Tissue-resident macrophages mediate neutrophil recruitment and kidney injury in Shiga toxin-induced hemolytic uremic syndrome. *Kidney Int*. 2021;100:349–363.
58. Lennon R, Singh A, Welsh GI, et al. Hemopexin induces nephrin-dependent reorganization of the actin cytoskeleton in podocytes. *J Am Soc Nephrol*. 2008;19:2140–2149.
59. Bakker WW, Borghuis T, Harmsen MC, et al. Protease activity of plasma hemopexin. *Kidney Int*. 2005;68:603–610.
60. Cheung PK, Klok PA, Baller JF, Bakker WW. Induction of experimental proteinuria in vivo following infusion of human plasma hemopexin. *Kidney Int*. 2000;57:1512–1520.
61. Zhou XJ, Vaziri ND, Pandian D, et al. Urinary concentrating defect in experimental hemochromatosis. *J Am Soc Nephrol*. 1996;7:128–134.
62. Zhou XJ, Laszik Z, Wang XQ, et al. Association of renal injury with increased oxygen free radical activity and altered nitric oxide metabolism in chronic experimental hemosiderosis. *Lab Invest*. 2000;80:1905–1914.
63. Kallianpur AR, Bradford Y, Mody RK, et al. Genetic susceptibility to postdiarrheal hemolytic-uremic syndrome after Shiga toxin-producing *Escherichia coli* infection: a Centers for Disease Control and Prevention FoodNet Study. *J Infect Dis*. 2018;217:1000–1010.
64. Nielsen R, Christensen EI, Birn H. Megalin and cubilin in proximal tubule protein reabsorption: from experimental models to human disease. *Kidney Int*. 2016;89:58–67.
65. Dixon SJ, Lemberg KM, Lamprecht MR, et al. Ferroptosis: an iron-dependent form of nonapoptotic cell death. *Cell*. 2012;149:1060–1072.
66. NaveenKumar SK, SharathBabu BN, Hemshekhar M, et al. The role of reactive oxygen species and ferroptosis in heme-mediated activation of human platelets. *ACS Chem Biol*. 2018;13:1996–2002.
67. Ferraris V, Acquier A, Ferraris JR, et al. Oxidative stress status during the acute phase of haemolytic uraemic syndrome. *Nephrol Dial Transplant*. 2011;26:858–864.
68. Monnens L, Molenaar J, Lambert PH, et al. The complement system in hemolytic-uremic syndrome in childhood. *Clin Nephrol*. 1980;13:168–171.
69. Arvidsson I, Ståhl AL, Hedström MM, et al. Shiga toxin-induced complement-mediated hemolysis and release of complement-coated red blood cell-derived microvesicles in hemolytic uremic syndrome. *J Immunol*. 2015;194:2309–2318.
70. Morigi M, Galbusera M, Gastoldi S, et al. Alternative pathway activation of complement by Shiga toxin promotes exuberant C3a formation that triggers microvascular thrombosis. *J Immunol*. 2011;187:172–180.
71. Ståhl AL, Sartz L, Karpman D. Complement activation on platelet-leukocyte complexes and microparticles in enterohemorrhagic *Escherichia coli*-induced hemolytic uremic syndrome. *Blood*. 2011;117:5503–5513.